processes

MDPI

Article

Rheological Behavior of Oleic Acid–Iron Mineral Suspensions for Steel Rolling Oily Sludge: Effects of Mineral Type, Volume Fraction, and Particle Size

Zhigang Que [1,2,*], Haifang Li [1,2], Jinming Shi [1,2], Xianbin Ai [1,2], Haiwei Jiang [1,2], Fan Gu [1,2], Tonghui Deng [1,2], Yinxuan Fu [1,2], Xiaodi Cheng [1,2] and Rong Huang [1,2]

[1] Key Laboratory of Greenhouse Gas Accounting and Carbon Reduction of Jiangxi Province, Institute of Energy Research, Jiangxi Academy of Sciences, Nanchang 330096, China; haifangli@139.com (H.L.); shijinming0012@163.com (J.S.); axbjxas@163.com (X.A.); haiweij@126.com (H.J.); gufan_nc@vip.163.com (F.G.); dth323@foxmail.com (T.D.); fuyinxuan_2007@163.com (Y.F.); kampfer@zju.edu.cn (X.C.); huangrong6128@163.com (R.H.)
[2] Jiangxi Carbon Neutralization Research Center, Nanchang 330096, China
* Correspondence: quezhigang@126.com; Tel.: +86-791-8817-9836

Abstract

The apparent viscosity of the oil–solid interface in steel rolling oily sludge (SROS) is governed by the amount, identity, and size of solid particles. To decouple these factors, oleic acid was used as a model oil phase, and Fe, Fe_3O_4, and Fe_2O_3 were selected as representative iron-bearing minerals. The effects of mineral type, Fe_3O_4 volume fraction, and particle size on the rheological behavior of oleic acid–mineral suspensions were systematically investigated using a rotational rheometer. Pure oleic acid behaved as a Newtonian fluid (24.96 mPa·s), and all suspensions exhibited near-Newtonian behavior with flow indices close to unity (0.959–1.048) and small yield stresses; no shear thickening was observed. At a matched loading of 4 vol%, the apparent viscosity followed the order Fe_3O_4 > Fe > Fe_2O_3. Notably, the Fe_2O_3 system exhibited a viscosity almost identical to that of neat oleic acid, which indicates that the reactivity of the mineral surface towards the carboxyl group of oleic acid, and the resulting aggregation state, dictate the particle–oil coupling, rather than the degree of oxidation. Furthermore, the apparent viscosity increased monotonically with Fe_3O_4 volume fraction (2–6 vol%) and decreased with increasing particle size (Dv(50) = 13.3–29.2 μm). Interestingly, the yield stress was highest for the coarsest powder, revealing that the static network strength and steady-flow viscosity are controlled by different microstructural features. These findings provide a quantitative basis for interpreting the oil–solid contribution to the viscosity of iron-bearing sludges and for developing targeted viscosity-reduction strategies.

Keywords: steel rolling oily sludge; apparent viscosity; oleic acid; iron-bearing minerals; Herschel–Bulkley model; agglomeration state

Check for updates

Academic Editor: Hyun Wook Jung

Received: 7 September 2026
Revised: 2 November 2026
Accepted: 4 November 2026
Published: 7 November 2026

Copyright: © 2026 by the authors. Licensee MDPI, Basel, Switzerland. This article is an open access article distributed under the terms and conditions of the Creative Commons Attribution (CC BY) license.

1. Introduction

During the rolling of crude steel, friction between the rolls and the steel produces iron powders, which combine with waste oil and emulsified water to form steel rolling oily sludge (SROS), a complex emulsion [1]. Owing to its flammability, odor, and soil/groundwater contamination potential, SROS is classified as hazardous waste in China's National Hazardous Waste List [2,3]. Approximately 0.86 kg of SROS is generated per ton of steel [4]; SROS typically contains 30–70% grease, 10–50% water, and 15.5–40 wt% iron powders [5].

 https://doi.org/10.3390/pr14213606

The thermal behavior and pyrolysis products of SROS have also been investigated to understand its resource recovery potential [6]. The author's previous research identified long-chain fatty acids (oleic, palmitic, and stearic acid) as the main oil-phase components. The solid phase is primarily composed of Fe_3O_4, accompanied by minor amounts of metallic Fe and Fe_2O_3, with a total Fe element content of 66.089 wt%. The particle sizes of these solids are mainly distributed in the ranges of 0.02–10 μm and 100–2000 μm (average size of 503.622 μm) [7]. Similar to petrochemical sludge, whose oil phase contains hydrophobic hydrocarbons together with hydrophilic resins and asphaltenes [8], the resins and asphaltenes in SROS form a robust interfacial film with water that inhibits droplet coalescence and reduces fluidity [9], and they interact with inorganic substances (SiO_2, Al_2O_3, CaO) to form viscoelastic interfacial films [10,11], ultimately yielding a high-viscosity oil–water–solid mixture [12]. The abundant colloids and asphaltenes interweave with solid particles into a network structure [13], giving the sludge high viscosity and poor fluidity [14]. In SROS, the carboxyl groups of long-chain fatty acids are hydrophilic and iron-oxide-philic, readily forming oil–water and oil–solid interfaces, while iron-bearing minerals spontaneously adsorb onto the oil–water interface to form a rigid interfacial film [15,16], hindering droplet aggregation and producing a stable, high-viscosity three-phase emulsion. The oil–solid interface structure is therefore critical to the apparent viscosity of SROS. Previous studies show that the viscosity of solid suspensions increases with solid volume fraction and decreases with increasing particle size [17,18], that smaller nanoparticles raise the viscosity of nanofluids [19,20], and that higher solid-particle concentration and smaller particle size enhance the stability and viscosity of oil emulsions [21,22]. Nevertheless, the specific factors governing the apparent viscosity of the oil–solid interface in SROS remain unclear owing to its distinct composition and structure. In this study, oleic acid, the predominant oil-phase component of SROS, and the representative iron-bearing minerals Fe, Fe_3O_4, and Fe_2O_3 were selected to investigate how mineral type, proportion, and particle size affect the apparent viscosity of the oleic acid–mineral interface, and to clarify the mechanism by which iron-bearing minerals raise the apparent viscosity of the oil–solid interface, providing a theoretical basis for efficient viscosity reduction in SROS.

Because the present work is concerned with the oil–solid contribution alone, the experiments were deliberately restricted to dry, water-free oleic acid–mineral suspensions. The interfacial films formed by resins, asphaltenes and inorganic fines at the oil–water interface, which dominate the rheology of the real three-phase sludge, are therefore outside the scope of this study. The mixtures examined here should accordingly be read as a simplified two-phase model of the oil–solid part of SROS.

2. Materials and Methods

2.1. Materials

Previous characterization of SROS by our group revealed that its oil phase is dominated by long-chain fatty acids, chiefly oleic acid (OA), palmitic acid, and stearic acid, among which oleic acid is the most abundant, accounting for more than 40 wt% [5]. Oleic acid was therefore adopted as the model oil phase in this study and was obtained from Aladdin Biochemical Technology Co., Ltd. (Shanghai, China).

The solid phase in SROS consists primarily of Fe_3O_4, accompanied by minor amounts of metallic Fe and Fe_2O_3. As reported in our earlier study [7], the iron-bearing particles in raw SROS exhibit a wide and bimodal size distribution (mainly concentrated in 0.02–10 μm and 100–2000 μm), with an average particle size of 503.622 μm. However, for the systematic investigation in this study, commercially available chemical reagents of Fe, Fe_3O_4, and Fe_2O_3 with a narrower size distribution were selected to better control the particle

size variable, all of which were purchased from Aladdin Biochemical Technology Co., Ltd. (Shanghai, China).

The phase compositions of the three reagents were confirmed by X-ray diffraction (XRD), as shown in Figure S1, indicating that the main minerals are Fe, Fe_3O_4, and Fe_2O_3, respectively. Their particle size distributions were measured by a laser diffraction particle size analyzer (Figure S2), showing that the sizes are primarily in the range of 1–100 μm, with Dv(50) values of 5.51 μm, 13.3 μm, and 9.38 μm for Fe, Fe_3O_4, and Fe_2O_3, respectively. To ensure that the iron powder consisted primarily of metallic Fe and was not severely oxidized, X-ray photoelectron spectroscopy (XPS) and scanning electron microscopy coupled with energy-dispersive X-ray spectroscopy (SEM-EDS) analyses were performed. The results (Figures S3 and S4) confirm that the surface of the iron powder is predominantly metallic Fe. Furthermore, the specific surface areas of the Fe, Fe_3O_4, and Fe_2O_3 powders were measured by N_2 physisorption at 77 K, which were 0.2933 m^2/g, 0.8064 m^2/g, and 21.3986 m^2/g, respectively.

To investigate the effect of the Fe_3O_4 particle size on the rheological behavior of the oleic acid–Fe_3O_4 mixture, medium- and large-sized Fe_3O_4 reagents were also purchased from the same supplier. Their particle size distributions are provided in Figure S5, showing that their sizes are also primarily distributed between 1 and 100 μm, with Dv(50) values of 24.4 μm and 29.2 μm, respectively.

2.2. Methods

2.2.1. Preparation of Iron-Bearing Mineral and Oleic Acid Mixture

All mixtures were prepared on a volumetric basis. For a target particle volume fraction (ϕ), the required mass of the mineral powder (m_p) was calculated using the following equation:

$$m_p = \frac{\phi \cdot V_{\text{oleic}} \cdot \rho_p}{1 - \phi} \quad (1)$$

where V_{oleic} is the volume of oleic acid (100 mL), and ρ_p is the true density of the mineral powder (Fe: 7.87 g/cm^3; Fe_3O_4: 5.17 g/cm^3; Fe_2O_3: 5.24 g/cm^3; oleic acid: 0.895 g/cm^3).

The preparation followed a uniform protocol: the calculated mass of powder was added to 100 mL of oleic acid preheated to 20 °C in a double-walled beaker with a circulating water bath. Each suspension was then homogenized at 8000 r/min for 5 min using a high-speed dispersing homogenizer (FJ300-SL, Shanghai Huxi Industrial Co., Ltd., Shanghai, China).

This protocol was applied to prepare three series of mixtures:

(1) Mineral type series: Fe, Fe_3O_4, and Fe_2O_3 powders (small size grade) were individually dispersed at a fixed particle volume fraction of 4 vol%.

(2) Volume fraction series: Fe_3O_4 powder (small size grade) was dispersed at particle volume fractions of 2, 4, and 6 vol%.

(3) Particle size series: Fe_3O_4 powders of small, middle, and large size grades were dispersed at a fixed particle volume fraction of 4 vol%.

2.2.2. Rheological Behavior Test

The rheological behavior of iron-bearing mineral and oleic acid mixtures was analyzed with a rotational rheometer (HAAKE MARS40, Thermo Fisher Scientific, Karlsruhe, Germany), assembled with a parallel–plate system, and the test temperature was set at 25 °C. The effect of shear rate on the apparent viscosity and on the shear stress was measured. In the steady-state shear-rate sweep mode, the shear rate was varied from 0.1 to 1000 s^{-1}. The plate diameter was 35 mm and the measuring gap 1.0 mm, i.e., more than ten times the Dv(90) of the coarsest powder used (82.4 μm). Each sample was loaded once onto the plate, left to equilibrate at 25 °C for 5 min before being subjected to a continuous steady-state

shear-rate sweep from 0.1 to 1000 s^{-1}. No re-homogenization or shear-history resets were performed during the sweep. To ensure reproducibility, each condition was independently prepared from scratch and measured twice (independent replicates). The averaged value of the two independent measurements is reported. For every data point in the flow curves, the relative deviation between the two independent measurements was within 5%, indicating good reproducibility. Given the large number of data points in each flow curve (approximately 100 points per curve); the observed trends were highly consistent between the two independent measurements. Because this is an absolute geometry, the shear rate and shear stress reported here are true material functions of the suspension rather than instrument-dependent readings [23].

2.2.3. Optical Microscopy Observation

The microstructures of the prepared samples were characterized using a biological optical microscope (T1500, Tuohe, Shanghai, China). Prior to observation, a small aliquot of the sample was gently placed on a clean glass slide (thickness: 1.0–1.2 mm) and covered with a coverslip to form a uniform thin liquid film and prevent bubble formation. The slide was then fixed on the mechanical stage with the specimen centered over the light aperture. The objective lens was first lowered cautiously near the slide using the coarse adjustment knob (monitored from the side to avoid contact), and then fine-focused through the eyepiece until a clear image was obtained. Micrographs were captured at a magnification of 40× to evaluate the dispersion state and aggregation behavior of the particles.

3. Results and Discussion

3.1. Effect of Mineral Type on the Rheology of Oleic Acid–Mineral Suspensions

Figure 1 presents the apparent viscosity and shear stress of pure oleic acid (100 vol%) and of oleic acid containing 4 vol% of Fe, Fe_3O_4 or Fe_2O_3, measured at 25 °C between 0.1 and 1000 s^{-1}. Pure oleic acid gave a constant viscosity of 24.96 ± 0.07 mPa·s over the whole shear-rate range, with a shear stress strictly proportional to shear rate, i.e., ideal Newtonian behaviour. At the matched loading of 4 vol% the three suspensions followed the order OA–Fe_3O_4 > OA–Fe > OA–Fe_2O_3. The Fe_3O_4 system was clearly the most viscous, its apparent viscosity falling from 42.7 mPa·s at 10 s^{-1} to 34.2 mPa·s at 1000 s^{-1}, whereas the Fe system was almost independent of shear rate (30.3 to 30.0 mPa·s) and the Fe_2O_3 system (25.8 to 23.6 mPa·s) fell slightly below the neat acid above 100 s^{-1} (Figure 1a). The shear-stress curves (Figure 1b) were linear and passed through the origin, with slopes ordered Fe_3O_4 > Fe > Fe_2O_3 ≈ OA, so the differences between the systems lie in the magnitude of the stress response rather than in the shape of the flow curve.

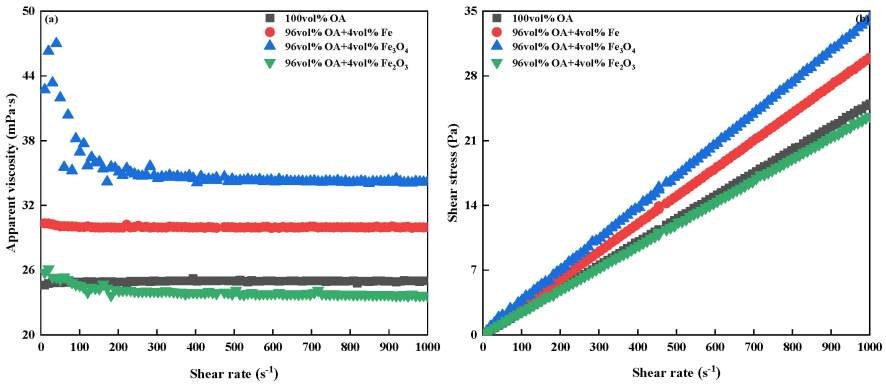

Figure 1. Apparent viscosity (**a**) and shear stress (**b**) of pure oleic acid and oleic acid systems containing 4 vol% Fe, Fe_3O_4, or Fe_2O_3 as a function of shear rate.

The steady-state shear-stress data of the four systems were fitted with the Herschel–Bulkley model [24] over the shear rate range of 10–1000 s^{-1}:

$$\tau = \tau_y + K\dot{\gamma}^n \quad (2)$$

where τ is the shear stress (Pa), τ_y is the yield stress (Pa), $\dot{\gamma}$ is the shear rate (s^{-1}), K is the consistency index (Pa·s^n), and n is the flow index.

For pure oleic acid, the fitting returned $\tau_y = 0$ Pa, $K = 0.02533$ Pa·s^n, and $n = 0.998$, indicating ideal Newtonian behavior with a viscosity equal to K. For the three suspensions, the fitted parameters were $\tau_y = 0.325$, 0.011, and 0.022 Pa, with $n = 1.005$, 1.001, and 0.989 for Fe_3O_4, Fe, and Fe_2O_3, respectively. Therefore, all four systems behave as essentially Newtonian fluids over the measured range, with the suspensions exhibiting only a small yield stress that grows with the strength of the particle network.

The ordering in Figure 1 follows from the particle–oil interface rather than from the amount of solid, which was identical in all three systems. Magnetite exposes both Fe^{2+} and Fe^{3+} sites and a correspondingly high density of surface hydroxyl groups, to which the carboxyl group of oleic acid can bind by coordination and ester-like condensation. The adsorbed layer thickens the effective particle and bridges neighboring particles into a network, which is why this system combines the highest viscosity with a yield stress an order of magnitude above the other two. Hematite (Fe_2O_3) is already fully oxidized and comparatively inert, so its particles interact only weakly with the oil and the viscosity remains close to that of the neat acid. The metallic iron surface, which typically carries a thin native oxide layer, exhibits an intermediate interfacial reactivity, resulting in a moderate viscosity increase. It should be noted that the three iron-based powders differ not only in surface chemistry but also in particle size and specific surface area. Their Dv(50) values are 5.51, 13.3, and 9.38 μm, and their BET surface areas are 0.2933, 0.8064, and 21.3986 m^2/g for Fe, Fe_3O_4, and Fe_2O_3, respectively. If these physical features were the dominant factors, the finest Fe powder (5.51 μm) or the Fe_2O_3 powder with the largest surface area (21.3986 m^2/g) should have exhibited the highest viscosity. However, the observed order (OA–Fe_3O_4 > OA–Fe > OA–Fe_2O_3) is completely decoupled from the size and surface area trends, strongly indicating that surface reactivity and the resulting aggregation state (as evidenced by Figure 2) are the primary factors dictating the apparent viscosity, while physical differences play only secondary roles.

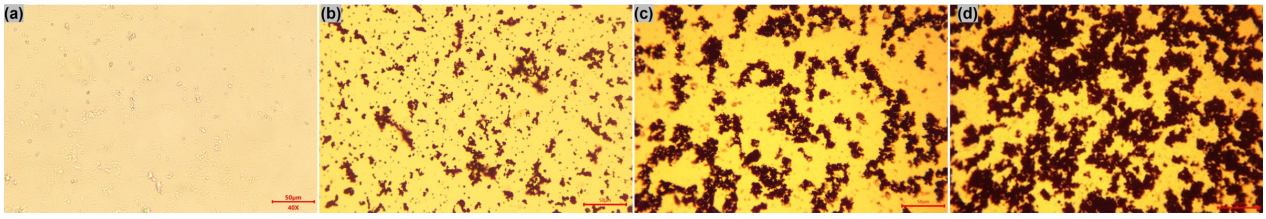

Figure 2. Microstructure of the mixture of oleic acid and iron-bearing minerals: (**a**) 100 vol% OA; (**b**) 96vol% OA + 4vol% Fe; (**c**) 96vol% OA + 4vol% Fe_3O_4; (**d**) 96vol% OA + 4vol% Fe_2O_3.

Figure 2 shows how the three powders are dispersed in the oil and provides direct support for this interpretation. Pure oleic acid (Figure 2a) was optically homogeneous. Fe particles (Figure 2b) remained largely as isolated units with only minor clustering, so the flow-unit size was changed comparatively little and the viscosity increase was modest. Both oxides agglomerated into flocculated networks (Figure 2c,d) but in different ways: Fe_3O_4 formed finer and far more numerous agglomerates that covered most of the field of view, whereas Fe_2O_3 formed coarser, more compact clusters separated by clear oleic acid. The finer, more extended Fe_3O_4 network immobilizes more of the continuous phase and provides more particle–particle contacts per unit volume, which is consistent with

the highest apparent viscosity and the largest yield stress of this system. In contrast, the compact Fe_2O_3 clusters leave most of the oil free to flow, producing a viscosity close to that of the neat acid.

3.2. Effect of Fe_3O_4 Volume Fraction on the Rheology of Oleic Acid–Fe_3O_4 Suspensions

Figure 3 shows the apparent viscosity and shear stress of OA–Fe_3O_4 mixtures prepared at Fe_3O_4 volume fractions of 2, 4 and 6 vol%. The apparent viscosity increased monotonically with loading: the steady-state averages over 10–1000 s^{-1} were 33.02, 35.18 and 38.55 mPa·s at 2, 4 and 6 vol%, i.e., 32%, 41% and 54% above the viscosity of pure oleic acid. The values at 100 s^{-1} were 34.10, 36.94 and 39.91 mPa·s. This is the behaviour expected of a well-dispersed suspension, in which the viscosity rises with the solids volume fraction [25,26], and the 2–6 vol% range studied here is too narrow for the pronounced curvature that appears as the maximum packing fraction is approached [27]. The yield stress increased in parallel, from 0.073 Pa at 2 vol% to 0.325 Pa at 4 vol% and 0.384 Pa at 6 vol%, so the additional solid is reflected both in the viscous response and in the strength of the particle network. The shear-stress curves in Figure 3b remained linear throughout, confirming that the near-Newtonian character is preserved at all three loadings.

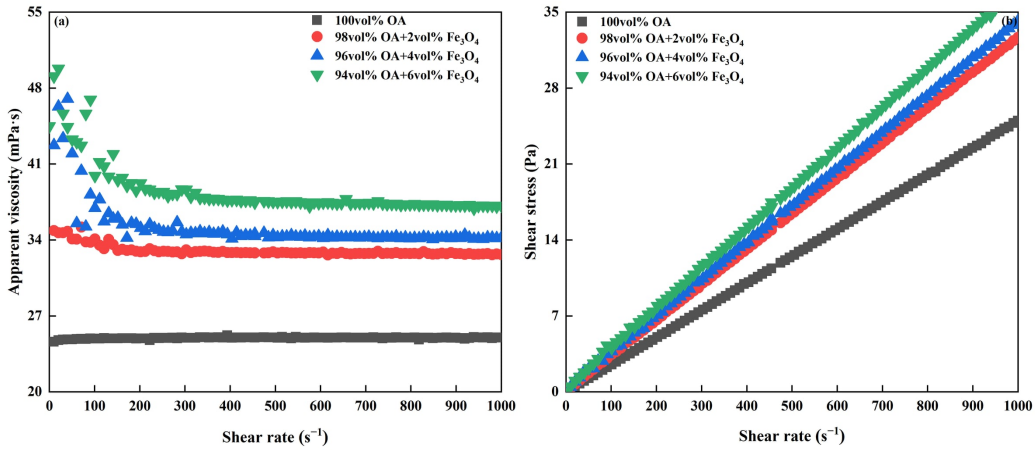

Figure 3. Apparent viscosity and shear stress of oleic acid–Fe_3O_4 mixtures at different volume proportions: (**a**) apparent viscosity; (**b**) shear stress.

Figure 4 shows the microstructures of the OA–Fe_3O_4 mixtures at 2, 4 and 6 vol%, together with pure oleic acid for reference (Figure 4a). The micrographs show a progressive increase in connectivity with loading, which is what produces the monotonic rise in viscosity described above: at 2 vol% the particles were present as comparatively isolated units with limited contact, at 4 vol% they had assembled into larger and better connected agglomerates, and at 6 vol% the network had become space-filling and continuous. The progressive build-up of a connected particle network is consistent with the simultaneous increase in the yield stress from 0.073 to 0.384 Pa.

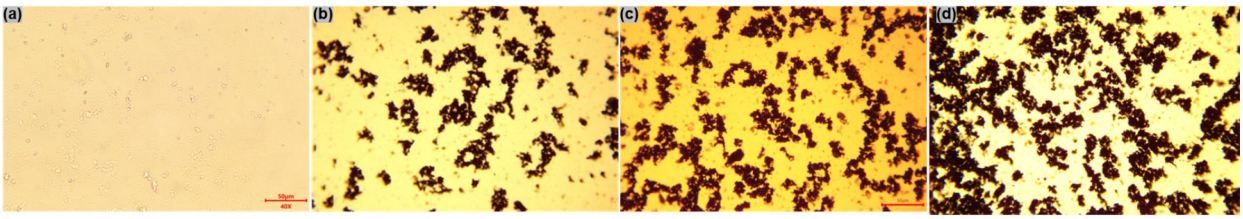

Figure 4. Microstructure of the oleic acid–Fe_3O_4 mixtures at different mineral volume proportions: (**a**) pure oleic acid; (**b**) 2 vol%; (**c**) 4 vol.%; (**d**) 6 vol%.

3.3. Effect of Particle Size on the Rheology of Oleic Acid–Fe_3O_4 Suspensions

Figure 5 shows the apparent viscosity and shear stress of OA–Fe_3O_4 mixtures prepared at a fixed loading of 4 vol% with Fe_3O_4 powders whose laser-diffraction median diameters were Dv(50) = 13.3, 24.4 and 29.2 μm for the small, middle and large grades. The apparent viscosity decreased monotonically with particle size: the steady-state averages over 10–1000 s^{-1} were 35.18, 27.94 and 27.48 mPa·s, i.e., +41%, +12% and +10% relative to pure oleic acid, and the values at 100 s^{-1} were 36.94, 28.26 and 31.79 mPa·s. This is the trend commonly reported for suspensions and nanofluids [28–30]: at a fixed volume fraction, finer particles give a larger number of particles and a larger total interfacial area per unit volume, and therefore a higher viscosity. The specific surface areas measured by N_2 physisorption (0.8064, 0.5569 and 0.5252 m^2/g for the three grades) are consistent with this interpretation. The yield stress, however, did not follow the same order: it was 0.325 Pa for the small powder, and decreased significantly to near zero (< 0.05 Pa) for the middle and large powders. The fine powder therefore owes its high viscosity and yield stress to the larger number of particle–oil contacts and the stronger, more extensive network, whereas the coarser powders form looser and weaker particle assemblies that offer less resistance to flow.

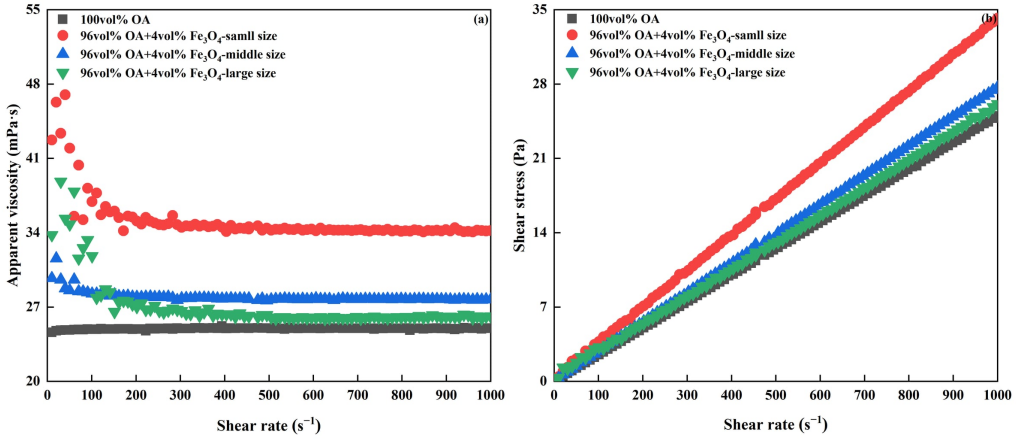

Figure 5. Apparent viscosity (**a**) and shear stress (**b**) of oleic acid–Fe_3O_4 mixtures at different particle sizes.

Figure 6 presents the microstructures of the OA–Fe_3O_4 mixtures prepared with the three Fe_3O_4 grades and explains the size dependence. The small-sized powder appeared as a dense distribution of fine units throughout the oil, the middle-sized powder formed more open, chain-like agglomerates, and the large-sized powder appeared as coarser, more isolated particles. The dense distribution of the fine powder gives the largest number of particle–oil contacts at a fixed volume fraction, consistent with its highest steady-state viscosity, whereas the open chains of the 25 μm powder give the weakest network and the lowest yield stress.

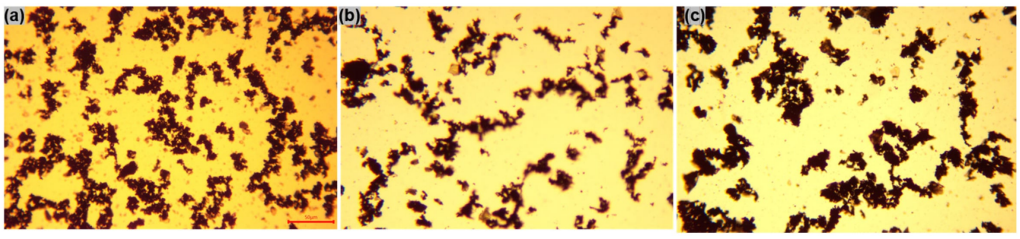

Figure 6. Microstructure of the oleic acid–Fe_3O_4 mixture at different particle sizes: (**a**) small size (Dv(50) = 13.3 μm); (**b**) middle size (24.4 μm); (**c**) large size (29.2 μm).

4. Conclusions

(1) Pure oleic acid is a Newtonian fluid ($\eta = 24.96 \pm 0.07$ mPa·s, $\tau_y = 0$, $n = 0.998$) over 0.1–1000 s^{-1} at 25 °C. All oleic acid–mineral suspensions examined were likewise near-Newtonian, being described by the Herschel–Bulkley model with $n = 0.959$–1.048, $R^2 \geq 0.9987$ and only a small yield stress. No shear thickening was observed over the whole shear-rate range.

(2) When compared at a matched particle volume fraction of 4 vol%, the apparent viscosity followed the order OA-Fe_3O_4 > OA-Fe > OA-Fe_2O_3, with the latter being almost identical to that of pure oleic acid. This viscosity order is not dictated by the degree of oxidation of the mineral, but rather by the surface reactivity towards the carboxyl group of oleic acid and the resulting aggregation state. Fe_3O_4 forms a finer and more extensive network that immobilizes the oil, whereas Fe_2O_3 forms dense, isolated clusters that leave most of the oleic acid free to flow.

(3) The apparent viscosity increased monotonically with the Fe_3O_4 volume fraction (33.02, 35.18 and 38.55 mPa·s at 2, 4 and 6 vol%) and exhibited an overall decreasing trend with particle size (35.18, 27.94 and 27.48 mPa·s at Dv(50) = 13.3, 24.4 and 29.2 μm). The yield stress decreased significantly with increasing particle size, dropping from 0.325 Pa for the fine powder to near zero for the coarser powders, so the strength of the static network and the steady-flow viscosity are controlled by different features of the particle assembly. Furthermore, it should be noted that this study focuses exclusively on the oil–solid interface. Because the model system contains no water, resins, or asphaltenes, these findings describe the oil–solid contribution to the apparent viscosity and should not be directly extrapolated to the complex three-phase SROS without further consideration.

Supplementary Materials: The following supporting information can be downloaded at: https://www.mdpi.com/article/10.3390/pr14213606/s1, Figure S1: XRD analysis of iron-bearing minerals: (a) Fe; (b) Fe standard (PDF# 06-0696); (c) Fe_3O_4; (d) Fe_3O_4 standard (PDF# 19-0629); (e) Fe_2O_3; (f) Fe_2O_3 standard (PDF# 33-0664); Figure S2: Size distribution of iron-bearing mineral; Figure S3: XPS spectra of the iron powder: (a) Survey scan; (b) High-resolution Fe 2p spectrum; Figure S4: SEM-EDS analysis of the iron powder: (a) SEM image; (b) EDS spectrum; Figure S5: Particle size distributions of Fe_3O_4 powders with different sizes.

Author Contributions: Conceptualization, Z.Q.; methodology, H.L., R.H., Y.F. and F.G.; software, T.D. and X.C.; validation, H.L. and Z.Q.; formal analysis, J.S. and X.A.; investigation, J.S.; resources, X.A.; data curation, T.D., R.H., Y.F., X.C., F.G. and H.J.; writing—original draft preparation, H.L., H.J. and Z.Q.; writing—review and editing, J.S. and Z.Q.; visualization, H.L., R.H. and Y.F.; supervision, J.S.; project administration, Z.Q.; funding acquisition, Z.Q. All authors have read and agreed to the published version of the manuscript.

Funding: This research was funded by the China Baowu Low-Carbon Metallurgy Innovation Foundation (No. BWLCF202316), the National Natural Science Foundation of China (No. 52364053), the Jiangxi Provincial Natural Science Foundation (No. 20252BAC220074), the Key R&D Program of Jiangxi Province (No. 20232BCJ23007 and 20233BCA01002), and Pilot Demonstration Project for the Contract Responsibility System of the Provincial Science and Technology Plan Project of Jiangxi Academy of Sciences (No. 2023YSTZX02).

Data Availability Statement: All data are available and can be shared upon request.

Conflicts of Interest: The authors declare no conflicts of interest.

References

1. Ge, L.; Mai, L.; Li, Q.; Rong, N.; Wang, Y.; Yang, Q.; Song, H.; Xu, C. Current research status and development trends in rolling oil sludge treatment. *Asia-Pac. J. Chem. Eng.* **2024**, *19*, e3135. [CrossRef]
2. Li, W.; Ma, Y.; Feng, X.; Alheshibri, M.; Bu, X.; Ma, G.; Ni, M.; Li, Q.; Liu, A.; Niu, X. Optimization of an oil recovery process from oily sludge using a combined technique of froth flotation and centrifugal treatment. *J. Clean. Prod.* **2023**, *400*, 136752. [CrossRef]
3. Ministry of Ecology and Environment of the People's Republic of China. *National Hazardous Waste List*; 2025 ed.; Ministry of Ecology and Environment of the People's Republic of China: Beijing, China, 2025. (In Chinese)
4. Qin, L.; Han, J.; He, X.; Zhan, Y.; Yu, F. Recovery of energy and iron from oily sludge pyrolysis in a fluidized bed reactor. *J. Environ. Manag.* **2015**, *154*, 177–182. [CrossRef]
5. Zhou, M.; Jiang, P.; Hu, Y.; Ali, M.-F.; Zhou, X. Study on the Formation Mechanism of Cold-Rolled Sludge and the Biodiesel Production from Sludge. *ACS Omega* **2023**, *8*, 35670–35681. [CrossRef]
6. Fu, Y.; Que, Z.; Shi, J.; Ai, X.; Zou, W. Thermal behavior and gas products of cold rolling oily sludge by TG-MS and Py-EGA/MS. *Energy Rep.* **2022**, *8*, 763–773. [CrossRef]
7. Que, Z.G.; Shi, J.M.; Fu, Y.X.; Ai, X.B.; Deng, T.H.; Huang, R. Basic characteristics of cold-rolling oily sludge and its oil and solid phases. *Appl. Chem. Ind.* **2023**, *52*, 665–670. (In Chinese)
8. Hassanzadeh, M.; Tayebi, L.; Dezfouli, H. Investigation of factors affecting on viscosity reduction of sludge from Iranian crude oil storage tanks. *Pet. Sci.* **2018**, *15*, 634–643. [CrossRef]
9. Zhang, J.; Tian, D.; Lin, M.; Yang, Z.; Dong, Z. Effect of resins, waxes and asphaltenes on water-oil interfacial properties and emulsion stability. *Colloids Surf. A* **2016**, *507*, 1–6. [CrossRef]
10. Souas, F. Rheological behavior of oil sludge from Algerian refinery storage tanks. *Pet. Res.* **2022**, *7*, 536–544. [CrossRef]
11. Liu, J.; Zhang, Y.; Peng, K.; Zhao, X.; Xiong, Y.; Huang, X. A review of the interfacial stability mechanism of aging oily sludge: Heavy components, inorganic particles, and their synergism. *J. Hazard. Mater.* **2021**, *415*, 125624. [CrossRef]
12. Huang, Q.; Han, X.; Mao, F.; Chi, Y.; Yan, J. A model for predicting solid particle behavior in petroleum sludge during centrifugation. *Fuel* **2014**, *117*, 95–102. [CrossRef]
13. Zadymova, N.M.; Skvortsova, Z.N.; Traskin, V.Y.; Yampol'skaya, G.P.; Mironova, M.V.; Frenkin, E.I.; Kulichikhin, V.G.; Malkin, A.Y. Heavy oil as an emulsion: Composition, structure, and rheological properties. *Colloid J.* **2016**, *78*, 735–746. [CrossRef]
14. Hu, J.; Gan, J.; Li, J.; Luo, Y.; Wang, G.; Wu, L.; Gong, Y. Extraction of crude oil from petrochemical sludge: Characterization of products using thermogravimetric analysis. *Fuel* **2017**, *188*, 166–172. [CrossRef]
15. Huang, Q.; Han, X.; Mao, F.; Chi, Y.; Yan, J. Effect of the particle surface on oil recovery from petroleum sludge. *Energy Fuels* **2014**, *28*, 4480–4485. Available online: https://pubs.acs.org/doi/abs/10.1021/ef500808x. [CrossRef]
16. Cano, M.; Sbargoud, K.; Allard, E.; Larpent, C. Magnetic separation of fatty acids with iron oxide nanoparticles and application to extractive deacidification of vegetable oils. *Green Chem.* **2012**, *14*, 1786–1795. [CrossRef]
17. Senapati, P.K.; Mishra, B.K.; Parida, A. Modeling of viscosity for power plant ash slurry at higher concentrations: Effect of solids volume fraction, particle size and hydrodynamic interactions. *Powder Technol.* **2010**, *197*, 1–8. [CrossRef]
18. Liu, F.; Xu, Q.; Qu, J.; Huang, Y.; Ma, J.; Lin, L. Effect of silica particle size on the viscosity, curing behavior, and sintering performance of silica/alumina ceramic suspensions for digital light processing-based vat photopolymerization. *Ceram. Int.* **2025**, *51*, 23459–23470. [CrossRef]
19. Rudyak, V.Y.; Dimov, S.V.; Kuznetsov, V.V. On the dependence of the viscosity coefficient of nanofluids on particle size and temperature. *Tech. Phys. Lett.* **2013**, *39*, 779–782. [CrossRef]
20. Yalçın, G.; Öztuna, S.; Dalkılıç, A.S.; Wongwises, S. The influence of particle size on the viscosity of water based ZnO nanofluid. *Alex. Eng. J.* **2023**, *68*, 561–576. [CrossRef]
21. Sullivan, A.P.; Kilpatrick, P.K. The Effects of inorganic solid particles on water and crude oil emulsion stability. *Ind. Eng. Chem. Res.* **2002**, *41*, 3389–3404. [CrossRef]
22. Zhao, H.; Yang, Y.; Chen, Y.; Li, J.; Wang, L.; Li, C. A review of multiple Pickering emulsions: Solid stabilization, preparation, particle effect, and application. *Chem. Eng. Sci.* **2022**, *248*, 117085. [CrossRef]
23. Stieger, M. The Rheology Handbook—For Users of Rotational and Oscillatory Rheometers. *Appl. Rheol.* **2002**, *12*, 232. [CrossRef]
24. Herschel, W.H.; Bulkley, R. Konsistenzmessungen von Gummi-Benzollösungen. *Kolloid-Z.* **1926**, *39*, 291–300. [CrossRef]
25. Krieger, I.M.; Dougherty, T.J. A mechanism for non-Newtonian flow in suspensions of rigid spheres. *Trans. Soc. Rheol.* **1959**, *3*, 137–152. [CrossRef]
26. Liu, T.; Hou, C.; Li, H.; Dahlen, P.; Guo, Y. The impact of solid particles and oil characteristics on the separation efficacy of oil sludge ultrasonic treatment. *Chem. Eng. Process.* **2024**, *205*, 109965. [CrossRef]
27. Zhang, T.; Zou, Q.; Cheng, Z.; Chen, Z.; Liu, Y.; Jiang, Z. Effect of particle concentration on the stability of water-based SiO2 nanofluid. *Powder Technol.* **2021**, *379*, 457–465. [CrossRef]
28. Timofeeva, E.V.; Smith, D.S.; Yu, W.; France, D.M.; Singh, D.; Routbort, J.L. Particle size and interfacial effects on thermo-physical and heat transfer characteristics of water-based α-SiC nanofluids. *Nanotechnology* **2010**, *21*, 215703. [CrossRef]

29. Hemmat Esfe, M.; Saedodin, S.; Wongwises, S.; Toghraie, D. An experimental study on the effect of diameter on thermal conductivity and dynamic viscosity of Fe/water nanofluids. *J. Therm. Anal. Calorim.* **2015**, *119*, 1817–1824. [CrossRef]
30. Özakın, B.; Gültekin, K.; Uğuz, G. Investigation of the Effect of Particle Size on Dispersion Stability and Viscosity in Kaolin Particles-Doped Bio-Based Palm Nanolubricants. *Arab. J. Sci. Eng.* **2025**, *50*, 4223–4241. [CrossRef]

Disclaimer/Publisher's Note: The statements, opinions and data contained in all publications are solely those of the individual author(s) and contributor(s) and not of MDPI and/or the editor(s). MDPI and/or the editor(s) disclaim responsibility for any injury to people or property resulting from any ideas, methods, instructions or products referred to in the content.